Electronic structure and optical properties of $(ZnS)_n/(Si_2)_m$ superlattices

E. G. Wang
Texas Center for Superconductivity and Space Vacuum Epitaxy Center, University of Houston, Houston, Texas 77204

C. S. Ting
Texas Center for Superconductivity and Department of Physics, University of Houston, Houston, Texas 77204
(Received 3 October 1994)

An approach has been suggested to integrate the superior properties of the ZnS semiconductor with the mature technology of Si. In a semiempirical tight-binding scheme, the detailed calculations of electronic structure and optical properties of the $(ZnS)_n/(Si_2)_m$ (110) superlattices are performed with a wide range of $n,m \leq 20$. A strong quantum confinement effect is found that causes the states at the conduction- and the valence-band edges confined in two dimensions in the Si wells. For a valence-band discontinuity $\Delta E_v = 1.9$ eV given by Harrison theory, the band gap between the confined band-edge states increases (2.37 eV at the $\bar{X}$ point for $n = m = 2$) by decreasing the superlattice period. An empty interface band is identified in the upper region of the gap, which extends over a quite different region of k space. The influence of valence-band discontinuity has been checked for all possible energy ranges. It is found that the dispersion and relative position of the interface band depend on valence-band discontinuity, but it does not disappear from the gap. Furthermore, the absorption spectra of the superlattices are calculated, which are found to be quite different from those of bulk ZnS and Si, but fairly close to their average.

I. INTRODUCTION

During the last few decades the potential for hybridization of compound semiconductors with silicon optoelectronics has led to significant efforts in optimizing the epitaxial growth on Si substrates.[1-4] For example, the successful growth of high quality GaAs on Si substrates[1,2] has many potential applications involving low-cost high-efficiency photovoltaics or large-scale integrated circuitry on a monolithic chip. However, GaAs is not a promising compound for epitaxial growth on Si, because of the large mismatches in both the lattice constants (4%) and thermal expansion coefficients (55%).[5] The residual strain results in structural defects such as dislocations, stacking faults, and microtwins, which have a detrimental effect on the optical and electronic properties of any device fabricated on the GaAs/Si system. As one of the most promising II-VI wide-band-gap compound semiconductors, ZnS not only has potential in the visible-to-ultraviolet range for optoelectronic device applications, but also matched lattice constants with Si, as the lattice mismatch between them is smaller than 0.4%.[6,7] A better approach, therefore, will be to integrate the superior properties of ZnS semiconductor with the mature technology of Si.

Up to the present, to our knowledge there has been no study which reports the band structures of $(ZnS)_n/(Si_2)_m$ superlattices over a wide range of n and m. The effects of the valence-band offsets ΔE_v on the band-gap and interface states in the ZnS/Si superlattice are not clear. It is not understood how the electronic and optical properties of $(ZnS)_n/(Si_2)_m$ superlattices change by varying the thickness of the epitaxial layers, which is interesting both for the basic research and for practical applications.

In this study, we will present our calculations for the (110) growth direction. The (110) interface is nonpolar in a lattice-matched system, while the (100) and (111) interfaces are polar interfaces. Some articles[8] have shown that, in a lattice-mismatched case, the atoms may no longer stay in planes perpendicular to the growth direction even for the (110) orientation. As a result this interface becomes slightly polar, which influences the band offset. The typical change of the (110) offsets are about 60–70 meV, induced by the out-of-plane motion in the ZnS/ZnSe system.[8] For the lattice-matched ZnS/Si superlattice, as shown in Fig. 1, the atoms at the interfaces stay in the interface planes. Therefore, it is reasonable to believe that the (110) interface is nonpolar. This is different from the case of the GaAs/Ge (100) superlattice,[9] which has two kinds of Ga-Ge and As-Ge abrupt planar interfaces (see Fig. 1 of Ref. 9); both Zn-Si and S-Si bonds here appear equally at the same interface of the ZnS/Si (110) superlattice, which leads each layer perpen-

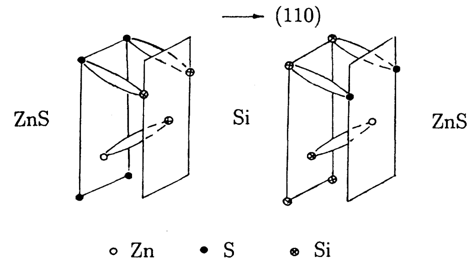

FIG. 1. Schematic interface bonding diagram of the ZnS/Si(110) superlattice.

 ©1995 The American Physical Society

dicular to the growth direction to be neutral. The interface electric fields deduced from the differences in the nuclear charges of the two kinds of interface atoms in a (100) or (111) growth direction will disappear in the present (110) growth case. In other words, the zero-field model[9–13] is well established for the lattice-matched ZnS/Si (110) superlattice.

The presentation is organized as follows. An outline of the tight-binding theory for the (110) growth superlattice is given in Sec. II, which also includes the band-structure fitting procedure for bulk ZnS and Si, as well as a discussion of the valence-band discontinuity between ZnS and Si, $\Delta E_v[=E_v(\mathrm{Si})\text{-}E_v(\mathrm{ZnS})]$. Section III gives the electronic properties of the superlattice, where we describe the calculated band structures, interface states, and energy gap between the confined band-edge states, and how they are affected by changes in ΔE_v. The optical property follows in Sec. IV. Section V contains a summary and our conclusions.

II. TIGHT-BINDING SCHEME

In the present calculation, a standard semiempirical sp^3s^* tight-binding method[14] has been employed. For each wave vector $\mathbf{k}$ in the Brillouin zone, the Bloch functions can be constructed by the linear combination of atomic orbitals $|\xi,\mathbf{r}_\alpha,\mathbf{R}_l\rangle$:

$$|\xi,\mathbf{r}_\alpha,\mathbf{k}\rangle=\frac{1}{\sqrt{N}}\sum_l e^{i\mathbf{k}\cdot\mathbf{R}_l+i\mathbf{k}\cdot\mathbf{r}_\alpha}|\xi,\mathbf{r}_\alpha,\mathbf{R}_l\rangle \ . \tag{2.1}$$

Here ξ is a quantum number that runs over the basis orbitals s, s^*, p_x, p_y, and p_z on the different types of sites α in a unit cell. The N wave vectors $\mathbf{k}$ lie in the first Brillouin zone with the origin of the lth unit cell at $\mathbf{R}_l$, and $\mathbf{r}_\alpha$ represents the positions of the atoms in this unit cell.

The electronic eigenstates of the superlattice are expanded as

$$\begin{aligned}|\mathbf{k},\lambda\rangle&=\sum_{\xi,\alpha}\langle\xi,\mathbf{r}_\alpha,\mathbf{k}|\mathbf{k},\lambda\rangle|\xi,\mathbf{r}_\alpha,\mathbf{k}\rangle\\&=\sum_{\xi,\alpha}C_{\xi\alpha}(\mathbf{k},\lambda)|\xi,\mathbf{r}_\alpha,\mathbf{k}\rangle \ .\end{aligned} \tag{2.2}$$

λ denotes the band index, and $C_{\xi\alpha}(\mathbf{k},\lambda)$ is the eigenwavefunction, which can be obtained by solving the Schrödinger equation

$$\sum_{\xi',\alpha'}[\langle\xi,\mathbf{r}_\alpha,\mathbf{k}|H|\xi',\mathbf{r}_{\alpha'},\mathbf{k}\rangle-E_\lambda(\mathbf{k})\delta_{\xi\xi'}\delta_{\alpha\alpha'}]\times\langle\xi,\mathbf{r}_\alpha,\mathbf{k}|\mathbf{k},\lambda\rangle=0 \ . \tag{2.3}$$

In this paper, only the nearest-neighbor interactions are included. Therefore, we obtain the Hamiltonian matrix for $(\mathrm{ZnS})_n/(\mathrm{Si}_2)_m$ (110) superlattices:

$$\langle\xi,\mathbf{r}_\alpha,\mathbf{k}|H|\xi',\mathbf{r}_{\alpha'},\mathbf{k}\rangle=\begin{array}{c|cccccccccccccccc} & 1 & 2 & 3 & 4 & & \cdots & m-1 & m & 1 & 2 & 3 & 4 & & \cdots & n-1 & n\\ \hline 1 & H_a & V_{ac} & 0 & U_{ac} & 0 & & & & & & \cdots & & & & 0 & U^+_{Ca}\\ 2 & & H_c & U_{ca} & 0 & 0 & & & & & & & & & & U^+_{Ac} & 0\\ 3 & & & H_a & V_{ac} & 0 & U_{ac} & & & & & & & & & & \\ 4 & & & & H_c & U_{ca} & 0 & 0 & & & & & & & & & \\ \vdots & & & & & & & \ddots & & & & & & & & & \\ m-1 & & & & & & & H_a & V_{ac} & 0 & U_{aC} & \ddots & & & & & \\ m & & & & & & & & H_c & U_{cA} & 0 & 0 & & & & & \vdots\\ 1 & & & & & & & & & H_b & V_{AC} & 0 & U_{AC} & & & & \\ 2 & & & & & & & & & & H_b & U_{CA} & 0 & 0 & & & \\ \vdots & & & & \mathrm{c.c} & & & & & & & & & \ddots & & & 0\\ & & & & & & & & & & & & & H_b & V_{AC} & 0 & U_{AC}\\ & & & & & & & & & & & & & & H_b & U_{CA} & 0\\ n-1 & & & & & & & & & & & & & & & H_b & V_{AC}\\ n & & & & & & & & & & & & & & & & H_b\end{array} \ , \tag{2.4}$$

where each element represents a 5×5 matrix. The diagonal elements H_j ($j=a$, b, and c) correspond to intrasite energies, and the others contain the nearest atomic interactions in the same layer (V_{ij}) or between two neighbor layers (U_{ij}) perpendicular to the growth direction. The superlattice consists of two different semiconductors labeled (a,c) for ZnS and (A,C) for Si, with a (110) interface. The terms a and c are regarded as the anion and cation atoms of the II-VI group compound semiconductor, while for convenience A and C are used to distinguish two kinds of atoms in silicon. Therefore, all elements in the Hamiltonian matrix are expressed as

$$H_{a(c)}=\begin{array}{c} \\ s \\ s^* \\ p_x \\ p_y \\ p_z \end{array}\begin{array}{c} \begin{array}{ccccc} s & s^* & p_x & p_y & p_z \end{array} \\ \left[\begin{array}{ccccc} E_s^{a(c)} & 0 & 0 & 0 & 0 \\ & E_{s^*}^{a(c)} & 0 & 0 & 0 \\ & & E_p^{a(c)} & 0 & 0 \\ & & & E_p^{a(c)} & 0 \\ & & & & E_p^{a(c)} \end{array}\right] \end{array}, \tag{2.5}$$

$$H_b=\begin{array}{c} \\ s \\ s^* \\ p_x \\ p_y \\ p_z \end{array}\begin{array}{c} \begin{array}{ccccc} s & s^* & p_x & p_y & p_z \end{array} \\ \left[\begin{array}{ccccc} E_s^{\mathrm{Si}} & 0 & 0 & 0 & 0 \\ & E_{s^*}^{\mathrm{Si}} & 0 & 0 & 0 \\ & & E_p^{\mathrm{Si}} & 0 & 0 \\ & & & E_p^{\mathrm{Si}} & 0 \\ & & & & E_p^{\mathrm{Si}} \end{array}\right] \end{array}, \tag{2.6}$$

$$V_{ac}=\begin{array}{c|ccccc} & s & s^* & p_x & p_y & p_z \\ \hline s & V_{(s,s)}P_1 & 0 & V_{(sa,pc)}P_2 & -V_{(sa,pc)}P_1 & 0 \\ s^* & 0 & 0 & V_{(s^*a,pc)}P_2 & -V_{(s^*a,pc)}P_1 & 0 \\ p_x & -V_{(sc,pa)}P_2 & -V_{(s^*c,pa)}P_2 & [V_{(x,x)}+V_{(x,y)}]P_1 & -V_{(x,y)}P_2 & 0 \\ p_y & V_{(sc,pa)}P_1 & V_{(s^*c,pa)}P_1 & -V_{(x,y)}P_2 & V_{(x,x)}P_1 & 0 \\ p_z & 0 & 0 & 0 & 0 & [V_{(x,x)}-V_{(x,y)}]P_1 \end{array}, \tag{2.7}$$

$$U_{ac}=\begin{array}{c|ccccc} & s & s^* & p_x & p_y & p_z \\ \hline s & V_{(s,s)}P_3 & 0 & 0 & V_{(sa,pc)}P_3 & V_{(sa,pc)}P_4 \\ s^* & 0 & 0 & 0 & V_{(s^*a,pc)}P_3 & V_{(s^*a,pc)}P_4 \\ p_x & 0 & 0 & [V_{(x,x)}-V_{(x,y)}]P_3 & 0 & 0 \\ p_y & -V_{(sc,pa)}P_3 & -V_{(s^*c,pa)}P_3 & 0 & V_{(x,x)}P_3 & V_{(x,y)}P_4 \\ p_z & -V_{(sc,pa)}P_4 & -V_{(s^*c,pa)}P_4 & 0 & V_{(x,y)}P_4 & [V_{(x,x)}+V_{(x,y)}]P_3 \end{array}, \tag{2.8}$$

$$U_{ca}=\begin{array}{c|ccccc} & s & s^* & p_x & p_y & p_z \\ \hline s & V_{(s,s)}P_5 & 0 & 0 & -V_{(sc,pa)}P_5 & V_{(sc,pa)}P_6 \\ s^* & 0 & 0 & 0 & -V_{(s^*c,pa)}P_5 & V_{(s^*c,pa)}P_6 \\ p_x & 0 & 0 & [V_{(x,x)}-V_{(x,y)}]P_5 & 0 & 0 \\ p_y & V_{(sa,pc)}P_5 & V_{(s^*a,pc)}P_5 & 0 & V_{(x,x)}P_5 & -V_{(x,y)}P_6 \\ p_z & -V_{(sa,pc)}P_6 & -V_{(s^*a,pc)}P_6 & 0 & -V_{(x,y)}P_6 & [V_{(x,x)}+V_{(x,y)}]P_5 \end{array}, \tag{2.9}$$

$$V_{AC}=\begin{array}{c} \\ s \\ s^* \\ p_x \\ p_y \\ p_z \end{array}\begin{array}{c} \begin{array}{ccccc} s & s^* & p_x & p_y & p_z \end{array} \\ \left[\begin{array}{ccccc} V_{s,s}P_1 & 0 & V_{s,p}P_2 & -V_{s,p}P_1 & 0 \\ 0 & 0 & V_{s^*,p}P_2 & -V_{s^*,p}P_1 & 0 \\ -V_{s,p}P_2 & -V_{s^*,p}P_2 & [V_{x,x}+V_{x,y}]P_1 & -V_{x,y}P_2 & 0 \\ V_{s,p}P_1 & V_{s^*,p}P_1 & -V_{x,y}P_2 & V_{x,x}P_1 & 0 \\ 0 & 0 & 0 & 0 & [V_{x,x}-V_{x,y}]P_1 \end{array}\right] \end{array}, \qquad (2.10)$$

$$U_{AC}=\begin{array}{c} \\ s \\ s^* \\ p_x \\ p_y \\ p_z \end{array}\begin{array}{c} \begin{array}{ccccc} s & s^* & p_x & p_y & p_z \end{array} \\ \left[\begin{array}{ccccc} V_{s,s}P_3 & 0 & 0 & V_{s,p}P_3 & V_{s,p}P_4 \\ 0 & 0 & 0 & V_{s^*,p}P_3 & V_{s^*,p}P_4 \\ 0 & 0 & [V_{x,x}-V_{x,y}]P_3 & 0 & 0 \\ -V_{s,p}P_3 & -V_{s^*,p}P_3 & 0 & V_{x,x}P_3 & V_{x,y}P_4 \\ -V_{s,p}P_4 & -V_{s^*,p}P_4 & 0 & V_{x,y}P_4 & [V_{x,x}+V_{x,y}]P_3 \end{array}\right] \end{array}, \qquad (2.11)$$

$$U_{CA}=\begin{array}{c} \\ s \\ s^* \\ p_x \\ p_y \\ p_z \end{array}\begin{array}{c} \begin{array}{ccccc} s & s^* & p_x & p_y & p_z \end{array} \\ \left[\begin{array}{ccccc} V_{s,s}P_5 & 0 & 0 & -V_{s,p}P_5 & V_{s,p}P_6 \\ 0 & 0 & 0 & -V_{s^*,p}P_5 & V_{s^*,p}P_6 \\ 0 & 0 & [V_{x,x}-V_{x,y}]P_5 & 0 & 0 \\ V_{s,p}P_5 & V_{s^*,p}P_5 & 0 & V_{x,x}P_5 & -V_{x,y}P_6 \\ -V_{s,p}P_6 & -V_{s^*,p}P_6 & 0 & -V_{x,y}P_6 & [V_{x,x}+V_{x,y}]P_5 \end{array}\right] \end{array}, \qquad (2.12)$$

where we have

$$P_1=\tfrac{1}{4}[e^{ibk_{xy}^-}+e^{-ibk_{xy}^+}] , \qquad (2.13)$$

$$P_2=\frac{\sqrt{2}}{4}[e^{ibk_{xy}^-}-e^{-ibk_{xy}^+}] , \qquad (2.14)$$

$$P_3=\tfrac{1}{4}e^{ibk_{zy}^+} , \qquad (2.15)$$

$$P_4=\frac{\sqrt{2}}{4}e^{ibk_{zy}^+} , \qquad (2.16)$$

$$P_5=\tfrac{1}{4}e^{ibk_{zy}^-} , \qquad (2.17)$$

$$P_6=\frac{\sqrt{2}}{4}e^{ibk_{zy}^-} , \qquad (2.18)$$

with

$$k_{xy}^{\pm}=\sqrt{2k_x}\pm k_y , \qquad (2.19)$$

$$k_{zy}^{\pm}=\sqrt{2}k_z\pm k_y , \qquad (2.20)$$

and

$$b=a_L/4 . \qquad (2.21)$$

a_L is the average of the cubic lattice constants of the bulk ZnS and Si.

The intramaterial elements in the Hamiltonian can be formed uniquely by using the corresponding bulk parameters. For the two intermaterial elements U_{aC} and U_{Ac} at the interface, a simple average of the bulk parameters has been used in the present calculations. These bulk parameters are determined by fitting the first-principles calculation. Yamaguchi's formula[15] has been adopted to yield self-consistent results at X-point energies. For example, the values of the energy of ZnS at high-symmetry points in the Brillouin zone are listed in Table I, which are in good agreement with the theoretical[16,17] and experimental[18–21] results. The calculated direct gap of ZnS is 3.79 eV. For Si our parameters given an indirect gap of 1.19 eV and a correct order of the conduction-band minima X-L-Γ.

Spin-orbit coupling is not included. Since the valence-band discontinuity of the ZnS/Si superlattice has not been established experimentally, we first assume the valence-band offset between ZnS and Si, $\Delta E_v[=E_v(\mathrm{Si})\text{-}E_v(\mathrm{ZnS})]$, to be 1.90 eV, which is the theoretical value given by Harrison,[22] and then study the effects of choice of ΔE_v in Sec. III D.

III. ELECTRONIC PROPERTY

A. Band structures

The band structure of the $(\mathrm{ZnS})_{16}/(\mathrm{Si}_2)_{16}$ (110) superlattice is displayed in Fig. 2, where the zero of energy

TABLE I. Comparison of various calculated and experimental data for ZnS (in eV). The top of the valence band (Γ_{15}^{v}) is chosen as the zero of energy.

Γ_1^v	Γ_1^c	Γ_{15}^c	
-12.89[a]	3.79[a]	8.00[a]	
-12.89[b]	2.26[b]	7.04[b]	
-11.7[c]	3.8[c]	8.0[c]	
-12.6[d]	3.7[d]	9.0[d]	
-13.5[e]	3.7[f]		
	3.85[g]		
X_5^v	X_1^c	X_3^c	
-2.10[a]	5.20[a]	5.70[a]	
-2.19[b]	3.61[b]	4.58[b]	
-1.6[c]	5.0[c]	6.0[c]	
-1.4[d]	5.7[d]	6.0[d]	
-2.5[e]			
L_1^v	L_3^v	L_1^c	L_3^c
-4.08[a]	-0.97[a]	4.45[a]	8.31[a]
-5.20[b]	-0.84[b]	3.65[b]	8.87[b]
-4.2[c]	-0.6[c]	5.0[c]	8.6[c]
-3.3[d]	-0.6[d]	5.3[d]	9.3[d]
-5.5[e]	-1.4[e]		

[a]Present work.
[b]Self-consistent linear combination of Gaussian orbitals method (Ref. 16).
[c]Self-consistent orthogonalized plane wave (Ref. 17).
[d]Korringa-Kohn-Rostoker (Ref. 18).
[e]X-ray photoemission spectroscopy (Ref. 19).
[f]Reflectivity at room temperature (Ref. 20).
[g]Reflectivity at 19 K (Ref. 21).

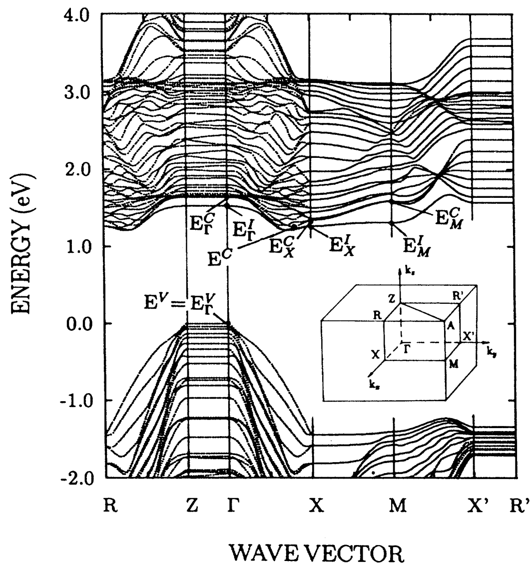

FIG. 2. Band structures of the $(ZnS)_{16}/(Si_2)_{16}$ (110) superlattice calculated by the first-neighbor sp^2s^* tight-binding method. The zero of energy corresponds to the top of the valence band of the superlattice. The inset shows the Brillouin zone of the $(ZnS)_n/(Si_2)_m$ (110) superlattice.

corresponds to the top of the valence band E^V $(=E_\Gamma^V)$ at $\mathbf{k}=0$. The inset shows the Brillouin zone of the $(ZnS)_n/(Si_2)_m$ (110) superlattice. The irreducible part is indicated with the labels of the eight symmetry points (R, Z, Γ, X, M, X', R', and A). It should be noted that the length of $\overline{\Gamma X}$ is not equal to that of $\overline{\Gamma X'}$ in the Brillouin zone of the (110) growth superlattice. The axis from the Γ point to the X point is normal to the projection of the Zn-Si and S-Si bonds on the (110) plane.

Because of the zone folding effect, the valence and conduction bands of the superlattice consist of many crowded subbands. The top of the valence band is shown by E^V in Fig. 2, which is located at the Γ point, and the bottom of the conduction band is shown by E^C located at $\tilde{X}$, which is near to the X point. The other lowest conduction band states are E_Γ^C, E_X^C, and E_M^C at the Γ, X, and M points, respectively. The large-band-gap ZnS layers cause quantum confinement in the small gap Si quantum wells. This superlattice has an indirect band gap of $E_g(E^C\text{-}E^V)=1.26$ eV, which is 0.07 eV larger than the band gap of the bulk Si (1.19 eV).

An empty interface band E^I in Fig. 2 was found lying below the conduction band. Different from the case of the GaAs/Ge(100) superlattice,[9] we do not find an occupied interface band above the valence band. We believe that the disappearance of the occupied band is due to the identical nonpolar interface in our (110) grown superlattice.

B. Confined states and interface states

The planar average of the charge densities of the band-edge states and the interface states for the $(ZnS)_{16}/(Si_2)_{16}$ (110) superlattice are shown in Figs. 3(a) and 3(b), respectively. All the band-edge states in Fig. 3 are confined in two dimensions in the Si well layers. Therefore, these states are believed to originate from those of Si by the zone folding effects. Furthermore, the occupancies on the confined states are distributed symmetrically, which shows that the interfaces at both sides of the Si layers are identical.

The interface states at Γ, X, and M have been analyzed in Fig. 3(b). These states are clearly localized on the interface. Because there is one kind of interface in the (110)-grown ZnS/Si superlattice, only one interface band is found in our study. We suggest that two interface bands corresponding, respectively, to Zn-Si and S-Si interfaces will be observed in a (100)-grown ZnS/Si superlattice. From Fig. 2 we see that the band of the interface state extends over a quite different region of k space.

C. Energy gap

Our calculated energy gap of the $(ZnS)_n/(Si_2)_m$ (110) superlattices as a function of $n=m$, shown as curve joining the discrete points at even integer values of n, are given in Fig. 4. In the same figure, the interface band E^I (dashed line) at the X point are also plotted. The theory shows that the lowest transition is the indirect Γ to $\tilde{X}$, which is near to the X point for all cases.

To illustrate quantum confinement, we also calculate

the energy gap for two different series of $(ZnS)_n/(Si_2)_m$ (110) superlattices, with $n=2$ as functions of m (Fig. 5), and with $m=2$ as functions of n (Fig. 6). The fundamental band gap of the superlattice, corresponding to the gap between the Si valence-band maximum and the Si folded conduction-band minimum, decreases as the Si layer thickness increases (Fig. 5). This effect becomes most dramatic, as expected, by varying m. When the Si layer thickness is fixed at 7.67 Å (four Si atoms thick), we find that the energy gap of the superlattice increases slowly as n changes from 2 to 20. It shows that the thickness of Si plays an important role in the formation of the fundamental band gap of the superlattice.

D. Effect of band offset

Since the value of the valence-band offset of ZnS/Si superlattices has not been reported experimentally, in the above calculations we adopt $\Delta E_v = 1.90$ eV, the theoretical value of Harrison based on the universal parameter tight-binding method.[22] In this section, we vary ΔE_v as a parameter to check how the result of the band-structure calculation is affected by the choice of ΔE_v.

There are two models shown here: (i) When the valence-band offset is less than 2.60 eV, the conduction-band minima of Si will lie below those of ZnS (type-I alignment). (ii) For an offset greater than 2.60 eV, the conduction-band alignment will be type II, with the superlattice conduction-band minimum being ZnS like. In Fig. 7, we show band structures of the $(ZnS)_{10}/(Si_2)_{10}$ (110) superlattice as $\Delta E_v = 1.5$, 1.9, 2.5, and 3.0 eV, respectively. For the type-I band alignment, the conduction-band minimum E^C is located at $\tilde{X}$ near the X point, which is formed by the zone folding effects from the conduction-band minima states of Si. The conduction-band minimum E^C of the superlattice moves to the Γ point in a band alignment with type-II, which originates from ZnS.

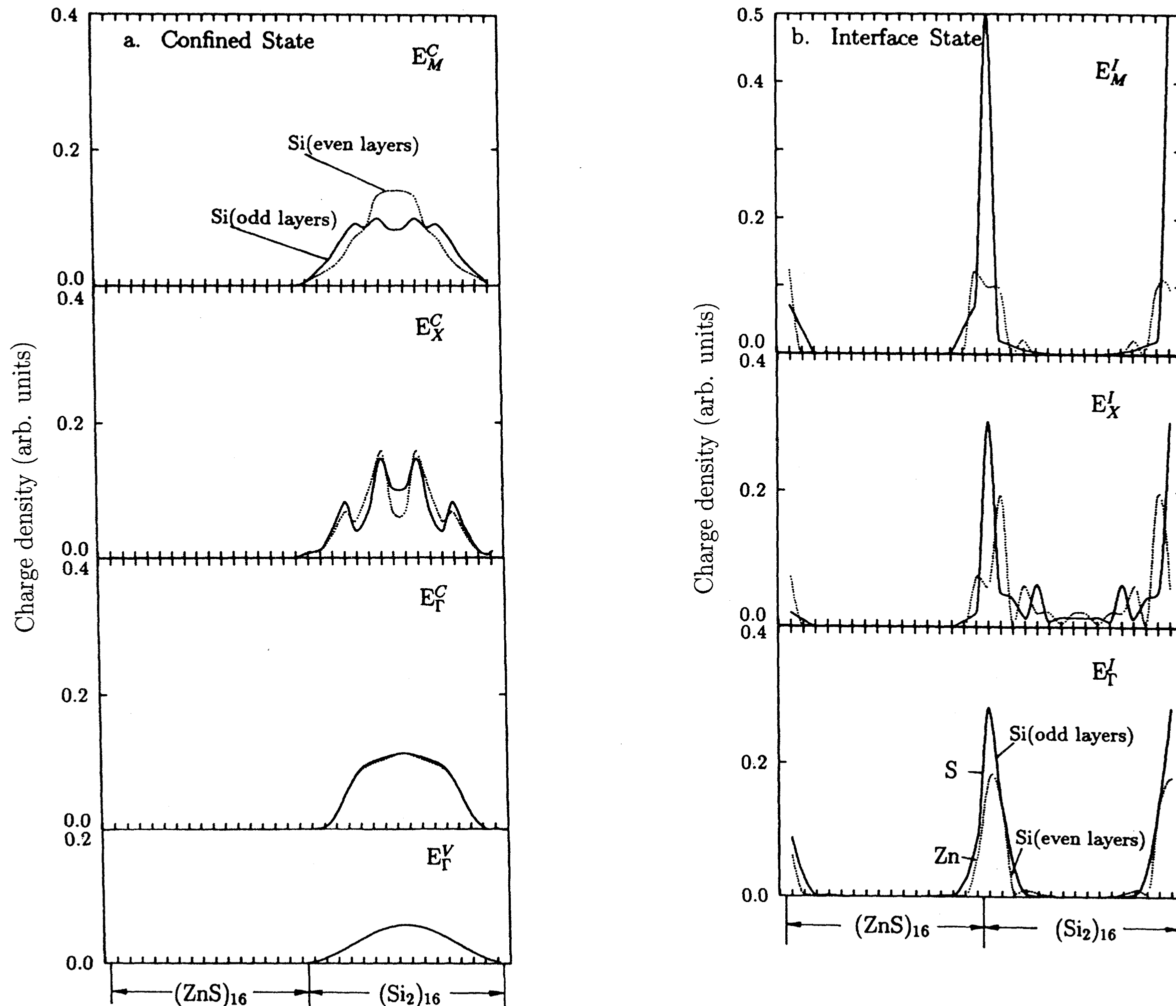

FIG. 3. Charge densities in the $(ZnS)_{16}/(Si_2)_{16}$ (110) superlattice. (a) The confined states; the occupied state (E_Γ^V) and the empty states (E_Γ^C, E_X^C, and E_M^C). (b) The interface states; the empty states (E_Γ^I, E_X^I, and E_M^I). The dashed lines indicate charge densities on the Zn and even-numbered Si layers, the solid lines those on the S and odd-numbered Si layers.

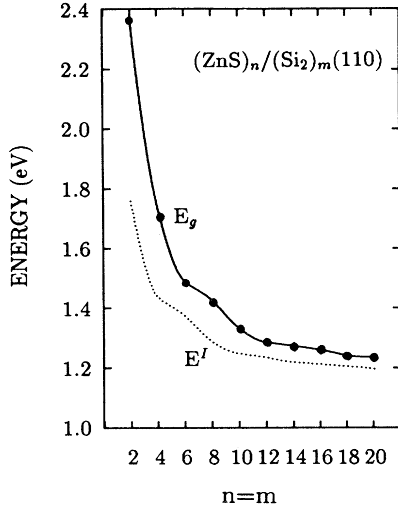

FIG. 4. Band gap E_g of $(ZnS)_n/(Si_2)_m$ (110) superlattices as a function of the number of layers $n=m$. The relative positions of the interface band E^I at the X point are also drawn in the same figure. The zero of energy is the valence-band maximum of the superlattice, and the assumed valence-band offset is 1.9 eV.

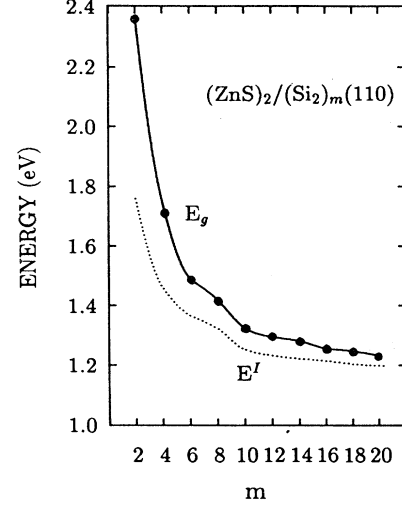

FIG. 5. Band gap E_g of $(ZnS)_n/(Si_2)_m$ (110) superlattices with $n=2$ as a function of the number of Si layers. The notations for the interface band and the valence-band offset are the same as those in Fig. 4.

A detailed description of the energy gap of the $(ZnS)_{10}/(Si_2)_{10}$ (110) superlattice as a functions of ΔE_v is shown in Fig. 8. The range of ΔE_v in this figure, 0.0–3.6 eV, covers all possible results. It is found that the largest indirect energy gap (1.43 eV) of the superlattice, with $n=m=10$, can be achieved by choosing $\Delta E_v=1.0$ eV. Continuously increasing ΔE_v, the superlattice experiences an indirect-direct-band-gap transition, with the energy decreasing from 1.43 to 0.88 eV. We do not believe that a $(ZnS)_{10}/(Si_2)_{10}$ (110) superlattice with a direct gap of 0.88 eV ($\Delta E_v=3.5$ eV) is a real structure fabricated by molecular-beam epitaxy (MBE) or other growth technology. As we see, the superlattice energy gap in this case is even smaller than that of Si (1.19 eV). When $\Delta E_v=3.0$ eV, the direct energy gap is 1.24 eV.

Furthermore, Fig. 8 shows that the relative position of the interface state E^I at the X point in the gap shifts down after a maximum at $\Delta E_v=1.0$ eV with increasing ΔE_v. It does not disappear from the gap within the range examined. It is concluded that the relative position of the interface state in the gap depends on the choice of ΔE_v, but it is always present in the gap.

IV. OPTICAL TRANSITION

In the empirical tight-binding approach, a momentum matrix element can be written as

$$\mathbf{P}_{\lambda,\lambda'}(\mathbf{k},\mathbf{k}')=\langle \mathbf{k},\lambda|\mathbf{p}|\mathbf{k}',\lambda'\rangle = \frac{1}{N}\sum_{\xi,\xi',\alpha,\alpha'} C^*_{\xi\alpha}(\mathbf{k},\lambda)C_{\xi'\alpha'}(\mathbf{k}',\lambda')\sum_{l,l'} e^{i[\mathbf{k}'\cdot(\mathbf{R}_{l'}+\mathbf{r}_{\alpha'})-\mathbf{k}\cdot(\mathbf{R}_l+\mathbf{r}_\alpha)]}\langle \xi,\mathbf{r}_\alpha,\mathbf{R}_l|\mathbf{p}|\xi',\mathbf{r}_{\alpha'},\mathbf{R}_{l'}\rangle \ . \tag{4.1}$$

Because of the strongly localized atomic orbitals in the tight-binding model, the momentum matrix elements between atoms separated by more than first-neighbor distances can be neglected.[23] Therefore, Eq. (4.1) may be reduced to

$$\mathbf{P}_{\lambda,\lambda'}(\mathbf{k},\mathbf{k}')=\sum_{\xi,\xi',\alpha} C^*_{\xi\alpha}(\mathbf{k},\lambda)C_{\xi'\alpha(\tau_\alpha)}(\mathbf{k}',\lambda')\mathbf{p}_{\xi,\xi'}(\mathbf{k},\mathbf{k}';\alpha) \ , \tag{4.2}$$

where

$$\mathbf{p}_{\xi,\xi'}(\mathbf{k},\mathbf{k}';\alpha)=\frac{1}{\sqrt{N}}\sum_l e^{i[(\mathbf{k}'-\mathbf{k})\cdot(\mathbf{R}_l+\mathbf{r}_\alpha)+\mathbf{k}'\cdot\tau_\alpha]} \times\langle \xi,\mathbf{r}_\alpha,\mathbf{R}_l|\mathbf{p}|\xi',\mathbf{r}_\alpha+\tau_\alpha,\mathbf{R}_l\rangle \ . \tag{4.3}$$

Here τ_α is the position of the neighbor atoms.

The absorption coefficient of a superlattice is given by[23–25] (apart from a constant factor)

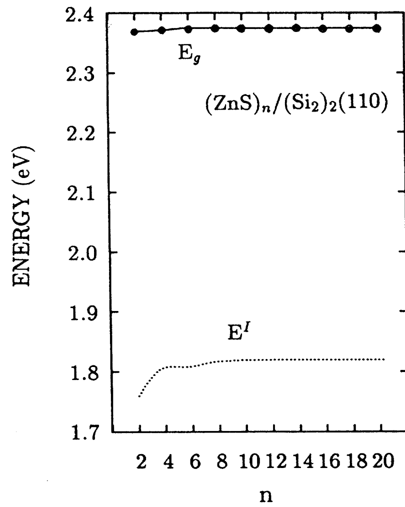

FIG. 6. Band gap E_g of $(ZnS)_n/(Si_2)_m$ (110) superlattices with $m=2$ as a function of the number of ZnS layers. The notations for the interface band and the valence-band offset are the same as those in Fig. 4.

$$\alpha(\hbar\omega)=\frac{1}{\omega}\sum_{\mathbf{k}}\sum_{\lambda\lambda'}|\epsilon\cdot\mathbf{P}_{\lambda,\lambda'}(\mathbf{k},\mathbf{k}')|^2 \times\delta[E_{\lambda'}(\mathbf{k})-E_{\lambda}(\mathbf{k})-\hbar\omega] \; . \quad (4.4)$$

The parameters $\langle \xi,\mathbf{r}_\alpha,\mathbf{R}_l|\mathbf{p}|\xi',\mathbf{r}_\alpha+\tau_\alpha,\mathbf{R}_l\rangle$ can be determined by comparing the theoretical computed values of bulks with their experimental results. The summations in Eq. (4.4) are over special points in the Brillouin zone. In our calculations, we took 28 special points in the $\frac{1}{8}$ two-dimensional Brillouin zone (k_x,k_y), and two special points in the $\frac{1}{2}$ one-dimensional Brillouin zone (k_z).[26] The calculated joint densities of states (JDOS) corresponding to the optical transitions[27,28] are given in Fig. 9 for $(ZnS)_n/(Si_2)_m$ (110) superlattices.

With increasing n $(=m)$, the absorption edge of ZnS/Si superlattices extends to lower energy (see Fig. 9). The curves rise rather slowly with some visible structures that may be related to critical-point transitions. Two main peaks are identified around 4.4 and 6.2 eV in all features. Compared with the absorption spectra of bulks, we note that the first peak originates from Si [4.2 eV (Ref. 28)], and the second from ZnS [6.0 eV (Ref. 29)].

V. CONCLUSION

In this paper, an approach has been suggested to integrate the superior properties of the ZnS semiconductor with the mature technology of Si. Detailed calculations of electronic structures and optical transitions for the $(ZnS)_n/(Si_2)_m$ (110) superlattices with a wide range of $n,m\leq 20$ are performed in a semiempirical tight-binding scheme. A quantum confinement effect is found that causes the states at the conduction- and valence-band edges to be confined to two dimensions in the Si wells. For a valence-band discontinuity $\Delta E_v=1.9$ eV given by

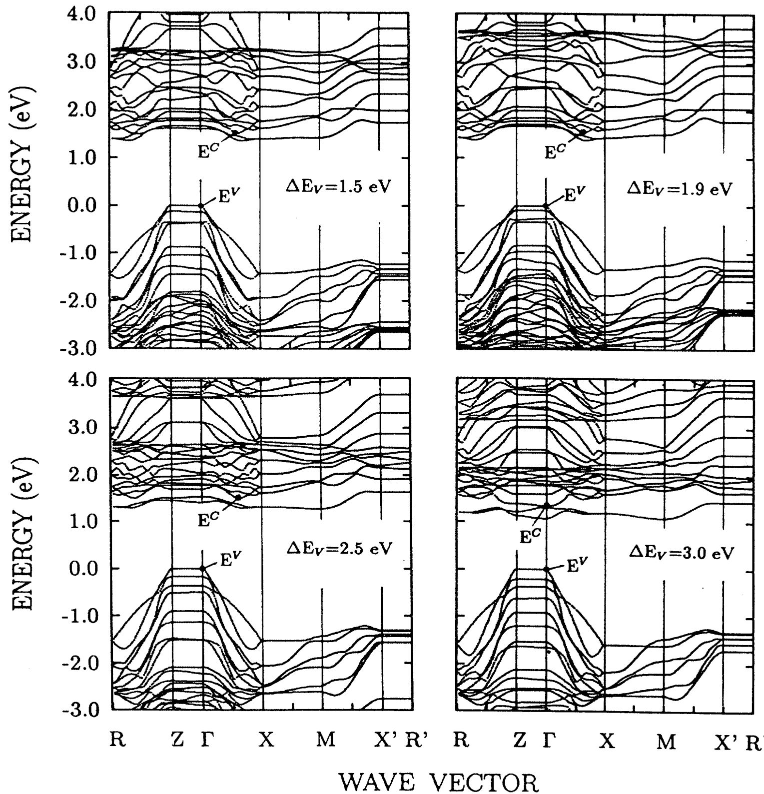

FIG. 7. Band structures of the $(ZnS)_{10}/(Si_2)_{10}$ (110) superlattice as $\Delta E_v=1.5$, 1.9, 2.5, and 3.0 eV, respectively. E^C and E^V, respectively, correspond to the bottom of the conduction band and the top of the valence band of the superlattice.

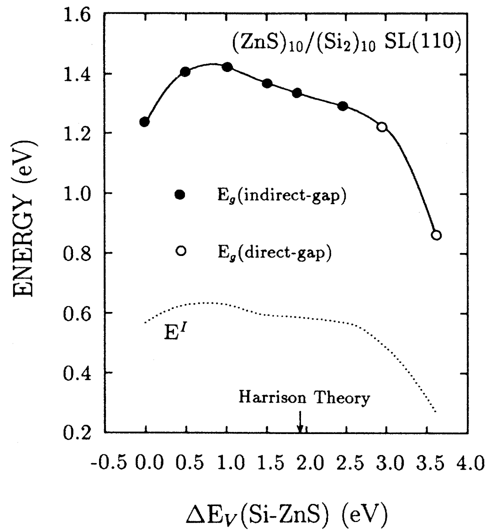

FIG. 8. Band gap (E_g) and related X-point interface state (E^I) of the $(ZnS)_{10}/(Si_2)_{10}$ (110) superlattices as functions of the valence-band discontinuity between ZnS and Si, ΔE_v.

Harrison theory, the band gap between the confined band-edge states increases (2.37 eV at the $\tilde{X}$ point for $n=m=2$) by decreasing the superlattice period. An empty interface band is identified in the upper region of the gap, which extends over a quite different region of k space. Since the value of the valence-band offset of the ZnS/Si superlattice has not been reported experimentally, two types of conduction-band alignments are examined by reasonable choices of ΔE_v for all possible energy values. We also show that the energy of the interface band depends on the valence-band discontinuity between ZnS and Si, but it does not disappear from the gap. Furthermore, joint densities of states of the superlattices are obtained which correspond to the optical transitions in these systems. The calculated absorption spectra are found to be quite different from those of bulk ZnS and Si, but fairly close to their average. Our results indicate that the optimal ZnS epilayers on the silicon substrate have a great deal of potential for optoelectronic device applications.

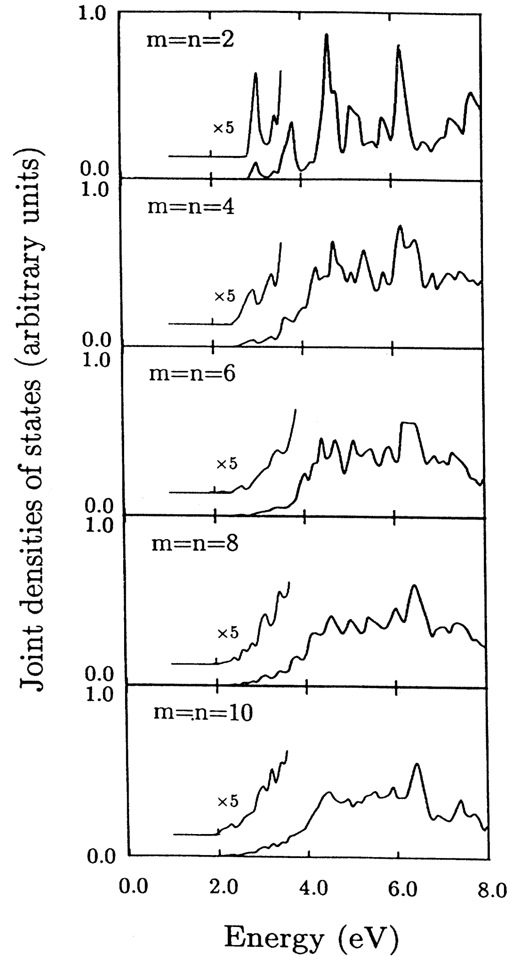

FIG. 9. Joint densities of states (JDOS) corresponding to the optical transitions for various $(ZnS)_n/(Si_2)_m$ (110) superlattices. The normalization is the same in all cases.

ACKNOWLEDGMENTS

The authors are grateful to Dr. X. Zhou for bringing our attention to this subject and for his interest. E. G. W. is indebted to Dr. J. H. Xu for his helpful discussions. The work was supported by the ARO Grant No. DAAH04-94-G-0075, and by the Texas Center for Superconductivity at the University of Houston.

[1]M. Akiyama, Y. Kawarada, and K. Kaminishi, J. Cryst. Growth **68**, 21 (1984).

[2]N. Chang, R. People, F. A. Baiochi, K. W. Wecht, and A. Y. Cho, Appl. Phys. Lett. **49**, 815 (1986).

[3]T. E. Crumbaker, H. Y. Lee, M. J. Hafich, and G. Y. Robinson, Appl. Phys. Lett. **54**, 140 (1989).

[4]O. Ueda, K. Kitahara, N. Ohtsuka, A. Hobbs, and M. Ozeki, in *Heteroepitaxy of Dissimilar Materials,* edited by R. F. C. Farrow, J. P. Harbison, P. S. Peercy, and A. Zangwill, MRS Symposia Proceedings No. 221 (Materials Research Society, Pittsburgh, 1991), p. 393.

[5]V. Alberts, J. H. Neethling, and A. W. Leitch, J. Appl. Phys. **75**, 7258 (1994).

[6]M. L. Cohen and T. K. Bergstresser, Phys. Rev. **141**, 789 (1966).

[7]H. Morkoç, S. Strite, G. B. Gao, M. E. Lin, B. Sverdlov, and M. Burns, J. Appl. Phys. **76**, 1363 (1994).

[8]N. E. Christensen and I. Gorczyca, Phys. Rev. B **44**, 1707 (1991).

[9]T. Saito and T. Ikoma, Phys. Rev. B **45**, 1762 (1992).

[10]J. Pollmann and S. T. Pantelides, Phys. Rev. B **21**, 709 (1980).
[11]E. Yamaguchi, J. Phys. Soc. Jpn. **57**, 2461 (1988).
[12]D. Shen, K. Zhang, and R. Fu, Appl. Phys. Lett. **53**, 500 (1988).
[13]J. Shen, J. D. Dow, and S. Y. Ren, J. Appl. Phys. **67**, 376 (1990).
[14]P. Vogl, H. P. Hjalmarson, and J. D. Dow, J. Phys. Chem. Solids **44**, 365 (1983).
[15]E. Yamaguchi, J. Phys. Soc. Jpn. **56**, 2835 (1987).
[16]C. S. Wang and B. M. Klein, Phys. Rev. B **24**, 3393 (1981).
[17]D. J. Stukel, R. N. Euwema, T. C. Collins, F. Herman, and R. L. Kortum, Phys. Rev. **179**, 740 (1969).
[18]P. Eckelt, O. Madelung, and J. Treusch, Phys. Rev. Lett. **18**, 656 (1967).
[19]L. Ley, R. A. Pollak, F. R. McFeely, S. P. Kowalczyk, and D. A. Shirley, Phys. Rev. B **9**, 600 (1974).
[20]M. M. Firsova, Fiz. Tverd. Tela (Leningrad) **16**, 54 (1974) [Sov. Phys. Solid State **16**, 35 (1974)].
[21]D. Theis, Phys. Status Solidi B **79**, 125 (1977).
[22]W. A. Harrison, J. Vac. Sci. Technol. **14**, 1016 (1977).
[23]Y. C. Chang and J. N. Schulman, Phys. Rev. B **31**, 2069 (1985).
[24]E. G. Wang, J. H. Xu, W. P. Su, and C. S. Ting, Appl. Phys. Lett. **64**, 443 (1994).
[25]E. G. Wang, W. P. Su, and C. S. Ting, J. Appl. Phys. **76**, 1 (1994).
[26]J. B. Xia and Y. C. Chang, Phys. Rev. B **42**, 1781 (1990).
[27]Zhizhong Xu, Solid State Commun. **76**, 1143 (1990).
[28]D. E. Aspnes and A. A. Studna, Phys. Rev. B **27**, 985 (1983).
[29]S. Ozaki and S. Adachi, Jpn. J. Appl. Phys. **32**, 5008 (1993).